Front-type solutions of fractional Allen-Cahn equation

Y Nec*, A A Nepomnyashchy * and A A Golovin†

*Department of Mathematics, Technion - Israel Institute of Technology, Haifa, 32000, Israel

† Department of Engineering Science and Applied Mathematics, Northwestern University, Evanston, Illinois, USA

Abstract Super-diffusive front dynamics have been analysed via a fractional analogue of Allen-Cahn equation. One dimensional kink shape and such characteristics as slope at origin and domain wall dynamics have been computed numerically and satisfactorily approximated by variational techniques for a set of anomaly exponents $1 < \gamma < 2$. The dynamics of a two dimensional curved front has been considered. Also, the time dependence of coarsening rates during the various evolution stages was analysed in one and two spatial dimensions.

PACS: 64.60.-i

Keywords: anomalous front, fractional Allen-Cahn equation, domain wall dynamics

1 Introduction

Reaction – diffusion equations govern numerous physical, chemical and biological systems [1, 2]. A characteristic feature of these systems is the multiplicity of stationary solutions and consequent existence of domain walls and fronts separating different states. An important distinction is that of fronts between locally stable states (e.g. interfaces developing due to phase separation) and fronts describing a replacement of an unstable state by a stable one (e.g. propagation of chemical reactions) [3, 1].

In the case of a reaction – diffusion equation for a single component

$$\partial_t u = \nabla^2 u + f(u), \tag{1}$$

the spatially homogeneous stationary states are determined by the zeros u_i of $f(u)$, while their stability depends on the sign of $f'(u_i)$. Applications of equation (1) include kinetics of phase transitions and chemical reactions. Paradigmatic examples of reaction – diffusion equations are Allen-Cahn equation [4] with $f(u) = u(1 - u^2)$, describing domain walls between two stable states ($u_1 = 1$ and $u_2 = -1$), and Fisher-Kolmogorov equation [5, 6] with $f(u) = u(1 - u)$, describing front propagation into an unstable state. Dynamics governed by (1) is characterised by the existence

*Tel.: 972-04-8294186; fax: 972-04-8293388. *E-mail address:* flyby@techunix.technion.ac.il

of Lyapunov functional

$$F\{u(x)\} = \int_{\mathbb{R}^d} \left(\frac{1}{2}(\nabla u)^2 - U(u) \right) d\mathbf{r}, \quad f(u) = U'(u), \tag{2a}$$

so that

$$\frac{dF}{dt} = -\int_{\mathbb{R}^d} \left(\frac{\partial u}{\partial t} \right)^2 d\mathbf{r} \leqslant 0. \tag{2b}$$

There exist physical systems subject to abnormally fast diffusion that can be described by means of a non-Gaussian random walk with algebraically decaying jump length distribution, also known as Lévy flight. Typical examples are wave turbulence [7], transport in porous media [8] and forage trajectories of animals [9]. For grounds, limitations and examples of such processes see review [10] and book [11]. Super-diffusion due to Lévy flights has been associated with reactive systems and transition between equilibrium states quite a while ago. An essential progress has been made recently in understanding the dynamics of *pulled* super-diffusive fronts propagating into an unstable state [12, 13, 14]. Fronts separating stable phases in systems with super-diffusion have been revealed studying transitions with long range interactions [15], vacancy diffusion and domain growth in binary alloys [16] and domain wall pinning by lattice defects [17].

The last example has touched on the topic of curvature reduction and coarsening of domain walls between competing phases (first modelled in [4] and known as Allen-Cahn mechanism) and associated that phenomenon with the time dependent Ginsburg-Landau equation. Still, to the authors knowledge, fronts between locally stable phases in systems with super-diffusion have not been studied systematically.

In the present paper a super-diffusive generalisation of (1) is considered

$$\partial_t u = \mathfrak{D}^{\gamma}_{|\mathbf{x}|} u + f(u), \tag{3a}$$

where

$$\mathfrak{D}^{\gamma}_{|\mathbf{x}|} = -\left(-\nabla^2\right)^{\gamma/2}, \quad 1 < \gamma < 2, \tag{3b}$$

is the fractional Laplacian, obtained as the macroscopic limit of Lévy type random walk [10]. A fractional analogue of Allen-Cahn equation is studied with the competing stable phases having an identical Lyapunov functional density. In section 2 the structure of motionless one dimensional domain wall between the phases is investigated. Section 3 is devoted to interaction of domain walls and simulation of the coarsening process. In section 4 a curved wall between the phases is considered, and finally competing stable phases of different Lyapunov functional values are studied in section 5.

2 Stationary solutions

A one dimensional fractional analogue of Allen-Cahn equation is analysed as the simplest model entailing diffusion anomaly effects on the phase separation transition

$$\partial_t u = \mathfrak{D}^{\gamma}_{|x|} u + u(1-u^2), \quad \mathfrak{D}^{\gamma}_{|x|} = -\frac{\sec(\pi\gamma/2)}{2\Gamma(2-\gamma)} \frac{d^2}{dx^2} \int_{-\infty}^{\infty} \frac{[\,\cdot\,]}{|x-\xi|^{\gamma-1}} d\xi. \tag{4}$$

2.1. Variational formulation

In order to evaluate the solutions of (4) it is useful to consider the following variational formulation. Define

$$\Upsilon(t) = \int_{-\infty}^{\infty} U(x,t)dx, \qquad U(x,t) = \frac{1}{4}(1-u^2)^2 - \frac{\sec(\pi\gamma/2)}{2\Gamma(2-\gamma)} \times$$
$$\left(\frac{\partial u}{\partial x} \frac{\partial}{\partial x} \int_{-\infty}^{\infty} \frac{u(\xi)}{|x-\xi|^{\gamma-1}} d\xi + \frac{u}{2} \int_{-\infty}^{\infty} \frac{\partial^2 u/\partial \xi^2}{|x-\xi|^{\gamma-1}} d\xi \right). \tag{5}$$

Then the first variation (denoted by δ) yields

$$\delta\Upsilon = -\int_{-\infty}^{\infty} (\mathfrak{D}^{\gamma}_{|x|} u + u - u^3)\delta u \, dx, \tag{6a}$$

$$\partial_t u = -\frac{\delta U}{\delta u} = \mathfrak{D}^{\gamma}_{|x|} u + u - u^3. \tag{6b}$$

Hence any solution of (4) will decay asymptotically to a stationary solution by

$$\partial_t \Upsilon = \int_{-\infty}^{\infty} \frac{\delta U}{\delta u} \partial_t u \, dx = -\int_{-\infty}^{\infty} (\partial_t u)^2 \, dx < 0. \tag{7}$$

Hereinafter the properties of such stationary solution are investigated.

2.2. Tail asymptotics

A brief summary of the basic properties of a normal stationary front $u(x)$ is brought for future comparison with the anomalous case. An exact solution of

$$u'' + u(1-u^2) = 0 \tag{8}$$

is given by

$$u(x) = s \, \tanh \frac{x - x_0}{\sqrt{2}}, \tag{9}$$

with $s = \pm 1$ and x_0 arbitrary. Later on the values $s = 1$ and $x_0 = 0$ are chosen so that $u(x)$ is odd. Since $u(\infty) = 1$, at $x \gg 1$ $u = 1 + \widetilde{u}$, $|\widetilde{u}| \sim o(1)$, where to leading order the *tail* $\widetilde{u}$ satisfies the linear equation

$$\widetilde{u}'' - 2\widetilde{u} = 0, \tag{10}$$

solved as

$$\widetilde{u} = c_1 e^{x\sqrt{2}} + c_2 e^{-x\sqrt{2}}. \tag{11}$$

Computing the deviation of (9) from the value at infinity,

$$\widetilde{u}(x) \sim -2e^{-x\sqrt{2}}, \quad x \to \infty. \tag{12}$$

The asymptotics at $x \to -\infty$ are similar as $u(x)$ is odd. The tail decay law is one of the front major characteristics, and as will be shown below, with the presence of anomaly it changes its nature from exponential to algebraic.

For the anomalous stationary front equation

$$\mathfrak{D}^{\gamma}_{|x|}u + u(1-u^2) = 0 \tag{13}$$

no exact solution is known, still it is possible to consider an odd solution satisfying $u(\pm\infty) = \pm 1$. It is expected that the essential change of $u(x)$ takes place in the region $|x| \sim O(1)$, whereas at $|x| \gg 1$ $u(x)$ tends to ± 1 asymptotically. The behaviour at $|x| \sim O(1)$ is treated in the next subsection. Hereby the tail asymptotics is sought by linearisation of (13) with $u = 1 + \widetilde{u}$, $|\widetilde{u}| \sim o(1)$, satisfying

$$\mathfrak{D}^{\gamma}_{|x|}\widetilde{u} - 2\widetilde{u} = 0, \quad x \gg 1. \tag{14}$$

To find Green's function for the operator $\mathfrak{D}^{\gamma}_{|x|} - 2$ the right-hand side of (14) is replaced by Dirac δ function

$$\mathfrak{D}^{\gamma}_{|x|}\widetilde{u} - 2\widetilde{u} = \delta(x), \tag{15}$$

and it is asserted that at infinity Green's function asymptotics coincides with that of the solution of (14) owing to the properties of δ function. Application of Fourier transform and rearranging yields

$$\mathcal{F}\widetilde{u}\,(q) = -\left(2 + |q|^{\gamma}\right)^{-1}. \tag{16}$$

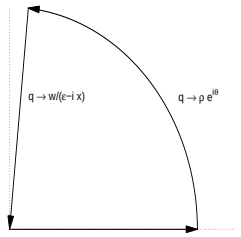

Figure 1: Modified integration path.

Bearing in mind that large x asymptotics corresponds to small q in Fourier space, (16) is expanded accordingly during Fourier transform inversion:

$$\widetilde{u}(x) = -\frac{1}{2\pi}\int_{-\infty}^{\infty}\frac{e^{iqx}}{2+|q|^{\gamma}}dq \sim -\frac{1}{4\pi}\lim_{\epsilon\to 0}\int_{-\infty}^{\infty} e^{iqx-\epsilon|q|}\left(1 - \frac{1}{2}|q|^{\gamma} + O(|q|^{2\gamma})\right)dq =$$

$$-\frac{1}{2}\delta(x) + \frac{1}{4\pi}\lim_{\epsilon\to 0}\int_{0}^{\infty} e^{-\epsilon q}\cos(qx)\left(q^{\gamma} + O(q^{2\gamma})\right)dq. \tag{17}$$

To evaluate the main contribution

$$I(x;\epsilon) = \Re\int_{0}^{\infty} e^{q(ix-\epsilon)}q^{\gamma}dq \tag{18}$$

a closed integration path is constructed (figure 1): along the arc $q = \rho\exp(i\theta)$ with $\mathbb{R} \ni \rho \to \infty$, $\theta \in [0\ \arctan(x/\epsilon)]$, and along the closing radius $q = w/(\epsilon - ix)$ with $w \in \mathbb{R}$. As the integrand of $I(x;\epsilon)$ is regular,

$$\lim_{\rho\to\infty}\left\{\int_{0}^{\rho} e^{q(ix-\epsilon)}q^{\gamma}dq + i\rho^{\gamma+1}\int_{0}^{\arctan(x/\epsilon)} e^{i\theta(\gamma+1)}e^{\rho(ix-\epsilon)\exp(i\theta)}d\theta + \right.$$

$$\left.(\epsilon - ix)^{-(\gamma+1)}\int_{\rho}^{0} e^{-w}w^{\gamma}dw\right\} = 0. \tag{19}$$

The integral along the arc is estimated as

$$\left|\int_0^{\arctan(x/\epsilon)} e^{i\theta(\gamma+1)} e^{\rho(ix-\epsilon)\exp(i\theta)} d\theta\right| = \left|\frac{-i}{\rho(ix-\epsilon)} \int_0^{\arctan(x/\epsilon)} e^{i\theta\gamma}\, d\, e^{\rho(ix-\epsilon)\exp(i\theta)}\right| \leqslant$$

$$\frac{1}{\rho\sqrt{x^2+\epsilon^2}} \left(e^{\rho(ix-\epsilon)\exp(i\theta)}\right)\Big|_0^{\arctan(x/\epsilon)},$$

vanishing under the limit $\rho \to \infty$. Hence

$$\widetilde{u}(x) \sim \tilde{p} x^{-(\gamma+1)} + O(x^{-(2\gamma+1)}), \quad \tilde{p} = -\frac{\sin(\pi\gamma/2)}{4\pi}\Gamma(\gamma+1). \tag{20}$$

Note also that functional (5) is convergent for functions of such asymptotics. In order to construct an approximation for the profile $u(x)$ in the entire domain $-\infty < x < \infty$ a shifted function $v = u - 1$ is defined. Substituting into (13) yields

$$\mathfrak{D}^{\gamma}_{|x|} v - 2v = 3v^2 + v^3. \tag{21}$$

Neglecting the detailed behaviour of $v(x)$ in the relatively thin region $|x| \sim O(1)$, the right-hand side of (21) is approximated by

$$\mathfrak{D}^{\gamma}_{|x|} v - 2v \approx 4\theta(-x), \tag{22}$$

with $\theta(x)$ being Heaviside step function. Differentiation with respect to x and comparison to (15) yields $v'(x) \sim -4\widetilde{u}(x)$ at $x \gg 1$. Returning to $u(x)$,

$$u(x) \sim 1 - 4\int_{\infty}^{x} \widetilde{u}(\xi) d\xi \sim 1 + p\, x^{-\gamma}, \quad p = -\frac{\sec(\pi\gamma/2)}{2\Gamma(1-\gamma)}, \quad x \gg 1. \tag{23}$$

Thus for an anomalous front an algebraic decay as γ-th power at infinity replaces the normal exponential one. Figure 2 compares asymptotics (23) with the numerical solution of (13), corresponding to a kink-antikink pair in a large domain. The deviation of the kink tail from the theoretical prediction at large distances from the kink center is caused by transition to the region where the second kink is situated.

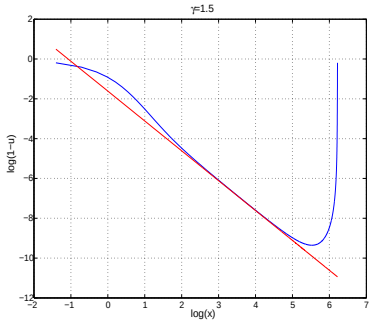

Figure 2: Comparison of asymptotic decay law (23) (straight line) with the numerical solution of (13).

2.3. Solution at $x \sim O(1)$

In order to calculate $u(x)$ for arbitrary values of x the variational formulation of the problem is used. Given the correct behaviour at infinity, an approximation is sought to the solution of (13) by minimisation of the time independent version of (5) through trial functions. For a set of values $1 < \gamma < 2$ the functional was computed with three kinds of trial functions combined with the algebraic tail: a simple polynomial, a sum of sines and an odd polynomial:

$$u_p(x) = \begin{cases} ax + bx^2 + cx^3 & 0 < x < \ell \\ 1 + px^{-\gamma} & x > \ell \end{cases} \tag{24a}$$

$$u_s(x) = \begin{cases} a\sin\left(\frac{x}{\ell}\right) + b\sin\left(\frac{2x}{\ell}\right) + c\sin\left(\frac{3x}{\ell}\right) & 0 < x < \ell \\ 1 + px^{-\gamma} & x > \ell \end{cases} \tag{24b}$$

$$u_{op}(x) = \begin{cases} ax + bx^3 + cx^5 & 0 < x < \ell \\ 1 + px^{-\gamma} & x > \ell\,. \end{cases} \tag{24c}$$

In all cases $u(-x) = -u(x)$. The functions u_s and u_{op} possess smooth derivatives at the origin, whereas $u_p(x)$ has a discontinuous second derivative. As is shown later, u_p is a good approximation despite this discontinuity. For Υ to exist the parameters a, b, c are chosen so that $u \in C^2$ on $(0, \infty)$. The principal value integrals in (5) are regularised accordingly in each case, and $\Upsilon(\ell;\gamma)$ is computed and minimised with respect to the juncture point $x = \ell$.

The computation of $\Upsilon(\ell;\gamma)$ is somewhat cumbersome, yet involves no special technique, and hence is not presented here. The resulting form is identical for all three functions:

$$\Upsilon(\ell;\gamma) = \sum_{j=0}^{4} K_j(\gamma)\ell^{1-j\gamma}, \tag{25}$$

with K_j being $\gamma-$dependent constants. Differentiating with respect to ℓ yields

$$\frac{d\Upsilon}{d\ell} = \ell^{-4\gamma}\sum_{j=0}^{4} K_j(1-j\gamma)\ell^{(4-j)\gamma}, \tag{26}$$

for which two positive roots are found: $\ell \to \infty$ and one root of the fourth degree polynomial, with the latter being the only minimum.

Figure 3 depicts the tails for a set of values of γ. It is seen that at γ close to normal the kink is steeper, whereas with further diminution of γ it is smoothed out. Away from the kink the deviation from the normal profile grows monotonously (and non-linearly) as γ decreases. The main difference between profiles obtained via trial functions of different types is the kink steepness: note that profiles generated by functions u_s (24b) and u_{op} (24c) are somewhat steeper for γ close to unity than those due to u_p (24a) (for instance scrutinise the distance along the x-axis where the value $u = 0.96$ is reached). With diminution of γ these differences become indistinct.

Equation (13) was also solved numerically by a pseudo-spectral code. Figure 4 compares the profiles obtained by the functional minimisation and direct numerical solution. Surprisingly, the solution with the lower degree polynomial trial function is the best evaluation of the three.

Figure 5 compares the functional value at the found minimum for the three trial functions and the numerical solution. Again, the third degree polynomial with its discontinuity in the second derivative at the origin gives a better result than the other two functions over most values of γ.

2.4. Validity of tail asymptotics

During the course of estimation of the front tail asymptotics the contribution of the kink core to the value of the decay constant p was neglected. To validate this step a posteriori a direct estimate is performed with the approximate solution $u_p(x)$ (24a).

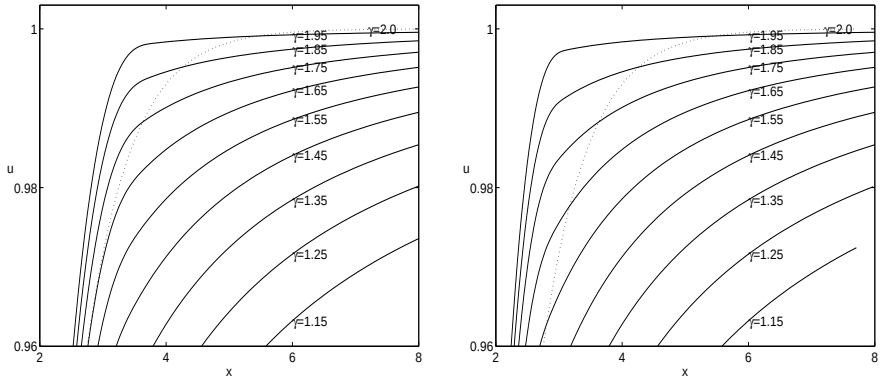

(a) Trial function $u_p(x)$ (24a)

(b) Trial function $u_s(x)$ (24b)

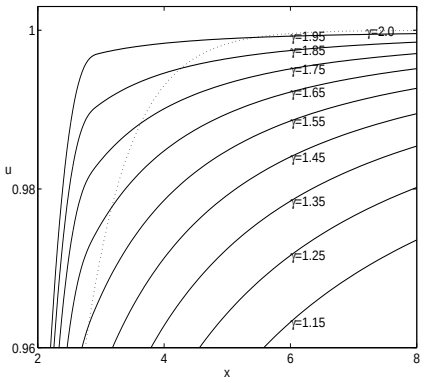

(c) Trial function $u_{op}(x)$ (24c)

Figure 3: Anomalous front profile tails.

The integration domain of $\mathfrak{D}^{\gamma}_{|x|}$ in (14) is divided into two sets $|\xi| < \ell$ and $|\xi| > \ell$. Omitting the prefacing factor,

$$\mathfrak{D}^{\gamma}_{|x|}u_p(x) = \frac{d^2}{dx^2}\left(\int_{|\xi|<x}\frac{u_p(\xi)d\xi}{(x-\xi)^{\gamma-1}} + \int_{|\xi|>x}\frac{u_p(\xi)d\xi}{|x-\xi|^{\gamma-1}}\right). \tag{27}$$

To compare the core and tail contributions $x > \ell$ is taken (with $\ell \sim O(1)$ being the juncture point between them, as determined by the functional minimisation) and the integrals in (27) are evaluated directly. The first integral consists of contributions of the inner $|\xi| < \ell$ and outer $\ell < |\xi| < x$ sets, whose respective magnitude is (after differentiation) $O(x^{-(\gamma+2)})$ and $O(x^{-\gamma})$. The contribution of the second integral is consistently $O(x^{-\gamma})$. Therefore the impact of the front core on the tail asymptotics is negligible at order $(-\gamma)$, and the constant p in the asymptotic decay law (23) is correct to that order. The effect of non-locality of $\mathfrak{D}^{\gamma}_{|x|}$ will manifest itself at order $-(\gamma+2)$.

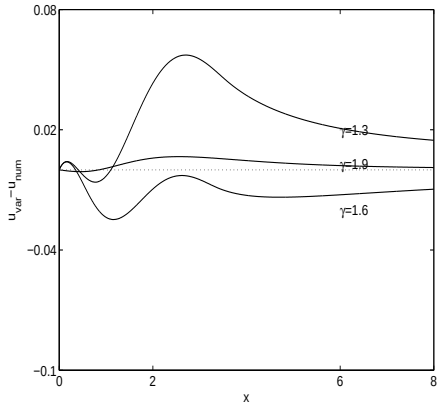

(a) Trial function $u_p(x)$ (24a)

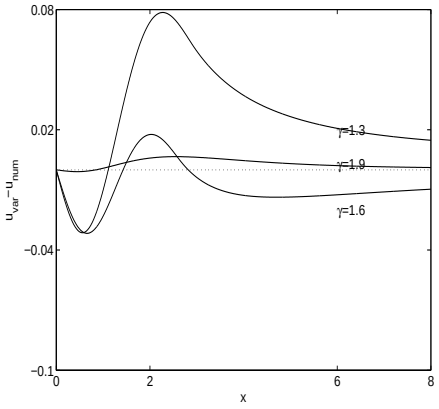

(b) Trial function $u_s(x)$ (24b)

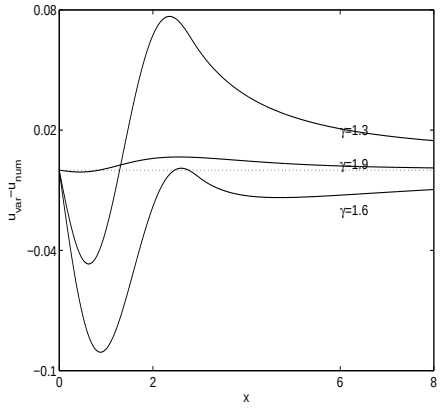

(c) Trial function $u_{op}(x)$ (24c)

Figure 4: Deviation of variationally and numerically obtained front profiles. The dotted curves show the deviation of the numerical solution for $\gamma = 2$ and the analytical profile (machine zero) $u(x) = \tanh(x/\sqrt{2})$.

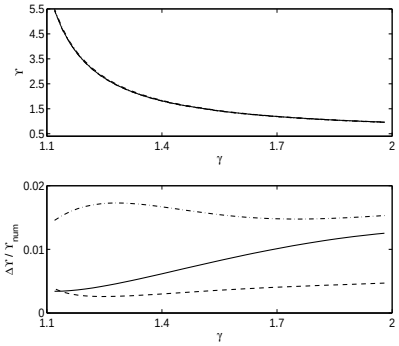

Figure 5: Upper: functional value for u_p ((24a), dashed), u_s ((24b), solid), u_{op} ((24c), dash-dotted) and the numerical solution (dotted) versus the anomaly exponent γ; lower: functional value difference relatively to the numerical solution for u_p (dashed), u_s (solid) and u_{op} (dash-dotted).

2.5. Anomaly dependent properties

Figure 6(a) depicts the front slope at the origin versus the anomaly exponent γ. For u_p (24a) the kinks become slightly less steep as γ decreases. The phenomenon is even more significant for u_{op} (24c), whereas for u_s (24b) the general trend is opposite. The slope of the normal profile is $\sqrt{2}/2$, so the curves can be considered upper and lower bounds for the slope of the true profiles.

Figure 6(b) shows the quantity $\int_{-\infty}^{\infty} u'^2 dx$ versus γ, corresponding to the inverse domain wall mobility (equalling $2\sqrt{2}/3 \approx 0.943$ for the normal profile). See the next section for details. The difference between the curves of u_p (24a) and u_s (24b) is practically independent of γ. On the other hand, u_{op} (24c) gives similar values for γ close to normal, but for decreasing γ its deviation becomes more significant.

Both the slope at origin and the inverse domain wall mobility are approximated best by u_p (24a), the lowest degree polynomial entailing a convergent functional.

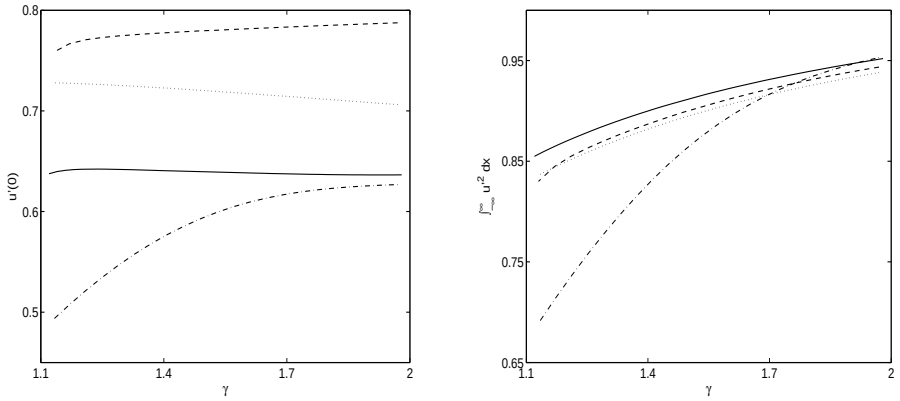

(a) Front slope at origin $u'(0)$ (b) Inverse wall mobility $\int_{-\infty}^{\infty} u'^2 dx$

Figure 6: Front properties versus anomaly exponent for u_p ((24a), dashed), u_s ((24b), solid), u_{op} ((24c), dash-dotted) and the numerical solution (dotted).

3 Dynamics of an ensemble of domain walls

In the course of phase segregation a number of domain walls are formed. The dynamics of an ensemble of domain walls in the case of normal Allen-Cahn equation was studied in [19, 20]. On late stages the coarsening is logarithmic, corresponding to the exponentially weak overlap of domain wall tails determined by the law (12). The present section is devoted to the dynamics of domain wall governed by (13).

3.1. *Dynamics of a pair of domain walls*

Consider two kinks moving in opposite directions, as in figure 7. A non-stationary correction satisfying

$$\partial_t u = \mathfrak{D}^{\gamma}_{|x|} u + u - u^3 \tag{28}$$

is sought by

$$u = u_0(x-\xi_1) - u_0(x-\xi_2) - 1 + \tilde{u}, \quad |\widetilde{u}| \ll 1, \tag{29}$$

where $u_0(x)$ is the solution of (13). Applying the shift $v := u - 1$ and defining $v_j(x) = (-1)^{j-1} u_0(x-\xi_j) - 1$, $j = \{1,2\}$,

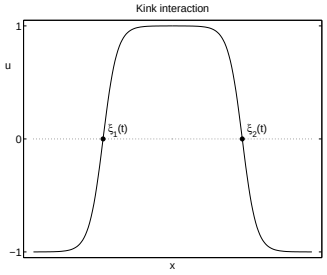

Figure 7: Kinks interaction.

$$v = v_1 + v_2 + \widetilde{v}, \quad |\widetilde{v}| \ll 1 \tag{30}$$

and should satisfy

$$\partial_t v = \mathfrak{D}^{\gamma}_{|x|} v - 2v - 3v^2 - v^3. \tag{31}$$

Defining a variable $\theta = x - \xi_1$, $|\theta| \ll 1$ about the core of the left kink, substituting (30) into (31) and neglecting all higher order terms according to

$$v_1 \sim O(1), \quad |\partial_t v_1| \ll 1, \quad \mathfrak{D}^{\gamma}_{|x|} v_j - 2v_j - 3v_j^2 - v_j^3 = 0, \tag{32a}$$

$$v_2 \sim -p(\xi_2 - x)^{-\gamma} \sim o(|v_1|), \quad \partial_t v_2 \sim o(|v_2|), \tag{32b}$$

yields

$$\left(\mathfrak{D}^{\gamma}_{|x|} - 2 - 6v_1 - 3v_1^2\right) \widetilde{v}(x) = -u_0'(x-\xi_1)\frac{d\xi_1}{dt} + \left(6v_1 + 3v_1^2\right) v_2(x), \tag{33}$$

or

$$\left(\mathfrak{D}^{\gamma}_{|\theta|} - 2 - 6v_1 - 3v_1^2\right) \widetilde{v}(\theta) = -u_0'(\theta)\frac{d\xi_1}{dt} + \left(6v_1(\theta) + 3v_1^2(\theta)\right) v_2(\theta), \tag{34}$$

with $v_1(\theta) = u_0(\theta) - 1$ and $v_2(\theta) = -u_0(\theta + \xi_1 - \xi_2) - 1$. The left-hand operator is self-adjoint, and the homogeneous adjoint problem

$$\left(\mathfrak{D}^{\gamma}_{|\theta|} - 2 - 6v_1 - 3v_1^2\right) \tilde{v}^c(\theta) = 0 \tag{35}$$

possesses a solution $\widetilde{v}^c(\theta) = v_1'(\theta) = u_0'(\theta)$ since by (32a)

$$\left(\mathfrak{D}^{\gamma}_{|\theta|} - 2 - 6v_1 - 3v_1^2\right) v_1'(\theta) = 0. \tag{36}$$

Thus by Fredholm alternative the solvability condition of (34) is

$$\int_{-\infty}^{\infty} {u_0'}^2(\theta) d\theta \; \frac{d\xi_1}{dt} = \int_{-\infty}^{\infty} \left[3\left(v_1^2(\theta)\right)' + \left(v_1^3(\theta)\right)'\right] v_2(\theta) d\theta. \tag{37}$$

Recognising

$$K = \int_{-\infty}^{\infty} {u_0'}^2(\theta) d\theta \tag{38}$$

as the inverse domain wall mobility, integrating by parts and applying the boundary conditions,

$$\frac{d\xi_1}{dt} = -\frac{1}{K}\int_{-\infty}^{\infty} \left(3v_1^2(\theta) + v_1^3(\theta)\right) v_2'(\theta) d\theta. \tag{39}$$

To obtain an approximation of (39),

$$3v_1^2 + v_1^3 \approx \begin{cases} 0 & x - \xi_1 \gg 1 \\ 4 & \xi_1 - x \gg 1 \end{cases}, \tag{40}$$

giving

$$\frac{d\xi_1}{dt} \approx \frac{4}{K}\int_0^{-\infty} v_2'(\theta) d\theta \sim \frac{\alpha}{K}(\xi_2 - \xi_1)^{-\gamma}, \quad \alpha = -4p > 0 \tag{41}$$

and similarly

$$\frac{d\xi_2}{dt} \sim -\frac{\alpha}{K}(\xi_2 - \xi_1)^{-\gamma}. \tag{42}$$

Figure 8 compares (39) integrated with variational (24a) and numerical profiles with asymptotics (41) and a direct numerical simulation of two kinks motion by (4). The differences between various computations emanate from the non-negligible deviation of the front core in the conforming profiles, as mobility is an integral property, yet the power law exponent is captured quite well for the entire range $1 < \gamma < 2$.

γ	slope
1.96	2.0
1.76	1.8
1.56	1.6
1.36	1.4
1.16	1.2

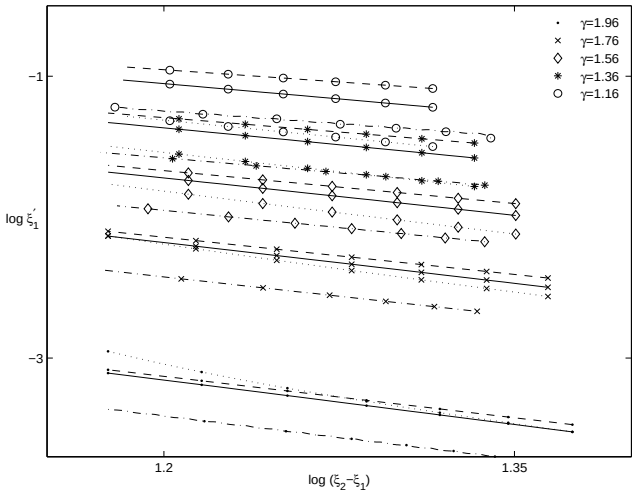

Figure 8: Evaluation of $d\xi_1/dt$ by numerical integration of (39) with variational $u_0(\theta) = u_p(\theta)$ (solid) and numerical (dotted) profiles, compared on a logarithmic scale with asymptotics (41) (dashed) and a direct numerical simulation of the motion of two kinks by (4) (dash-dotted). The approximate power law exponents are brought in the table (absolute values).

3.2. Dynamics of multiple domain walls

Equation (13) was solved numerically by means of a pseudo-spectral code with time integration in Fourier space, using Crank-Nicholson scheme for the linear operator and

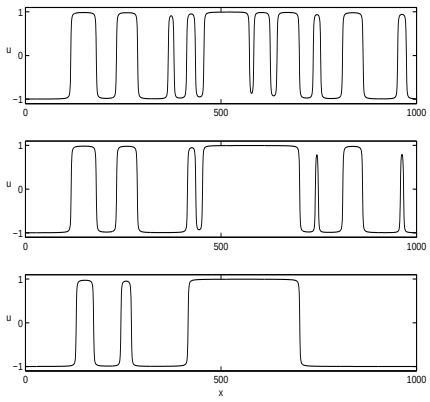

Figure 9: Coarsening of a system of multiple kinks for $\gamma = 1$.

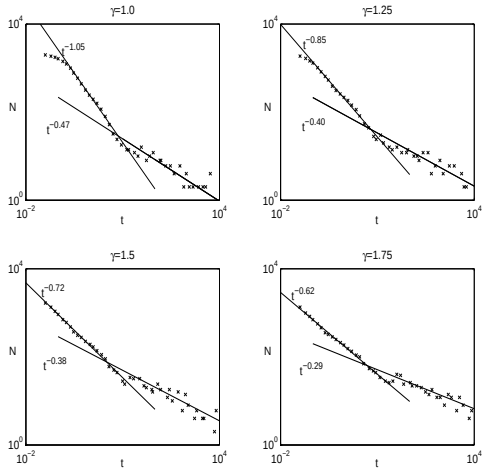

Figure 10: Coarsening rates of a system of multiple kinks for several values of γ.

Adams-Bashforth scheme for the non-linear one. Coarsening of a system of multiple kinks in a large domain was studied with periodic boundary conditions and random initial data. Snapshots of the coarsening kinks are shown in figure 9 for $\gamma = 1$.

The coarsening rates were measured for several values of γ by counting the number of zeros N of the function $u(x,t)$. The results of runs with random initial data are brought in figure 10. Two regimes are evident: (i) the initial regime corresponds to a linear growth of the initial data and formation of a system of kinks, as described by the linearised version of (13) that gives $N \sim t^{-1/\gamma}$; (ii) the crossover to kink annihilation and system coarsening. Indeed, the exponents presented in the figure are close to $1/\gamma$ during the first part of the evolution, and the coarsening exponents are close to $1/(2\gamma)$.

4 Two dimensional front properties

4.1. Analytical prediction

In a space of dimension d equation (4) becomes [21]

$$\partial_t u = \widetilde{\mathfrak{D}}^{\gamma}_{|\mathbf{x}|} u + u(1-u^2),$$

$$\widetilde{\mathfrak{D}}^{\gamma}_{|\mathbf{x}|} u(\mathbf{x},t) = -C_{d,\gamma/2} \int_{\mathbb{R}^d} \frac{u(\mathbf{x},t) - u(\boldsymbol{\xi},t)}{|\mathbf{x}-\boldsymbol{\xi}|^{d+\gamma}} d\boldsymbol{\xi}, \qquad (43a)$$

where

$$\widetilde{\mathfrak{D}}^{\gamma}_{|\mathbf{x}|} = -\left(-\nabla^2\right)^{\gamma/2}, \quad C_{d,\alpha} = \frac{2^{2\alpha}\Gamma(d/2+\alpha)}{\pi^{d/2}|\Gamma(-\alpha)|}. \qquad (43b)$$

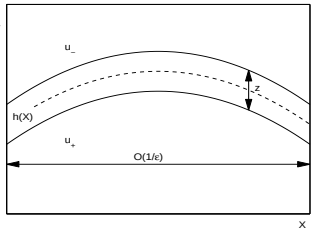

Figure 11: Curved front inner layer.

Suppose a two dimensional space consists of regions with $u \approx -1$, $u \approx 1$ and a transition between them in the form of a curved front, so that the front width is small and its radius of curvature is large compared to the size of the stable phases regions (figure 11). Slow spatial variables $X = \epsilon x$, $Y = \epsilon y$ will describe the front as an inner layer, whose velocity of order $O(\epsilon)$ in the original variables now becomes $O(\epsilon^2)$. Thus a slow temporal variable is $T = \epsilon^2 t$.

A detailed derivation appears in appendix A. To leading order the solution is

$$u_0(X,z,T) = u_{pf}(Z), \quad Z = \frac{z}{\sqrt{1+h_X^2}}, \qquad (44)$$

with u_{pf} being the plane front (13) stretched by the arc length of the curve $h(X)$. The correction equation is

$$\left(\left(1+h_X^2\right)^{\gamma/2} \widetilde{\mathfrak{D}}^{\gamma}_{|z|} + 1 - 3u_0^2\right) u_1 = -h_T u_{0z} + \gamma \left(1+h_X^2\right)^{\gamma/2-1} \times$$

$$\left(h_X \partial_z^{-1} \widetilde{\mathfrak{D}}^{\gamma}_{|z|} u_{0X} + \frac{h_{XX}}{2\left(1+h_X^2\right)} \left(1 + (\gamma-1)h_X^2\right) \partial_z^{-1} \widetilde{\mathfrak{D}}^{\gamma}_{|z|} u_0\right), \qquad (45)$$

and the conforming solvability condition is given by

$$K\, h_T = \frac{1}{2}\gamma\, M \frac{h_{XX}}{1+h_X^2},$$

$$K = \int_{\mathbb{R}} {u_0}'^2(Z) dZ, \quad M = -\int_{\mathbb{R}} u_0(Z) \widetilde{\mathfrak{D}}^{\gamma}_{|Z|} u_0(Z) dZ. \qquad (46)$$

The normal velocity v_n and the front curvature κ

$$v_n = \frac{h_T}{\sqrt{1+h_X^2}}, \quad \kappa = -\frac{h_{XX}}{\left(1+h_X^2\right)^{3/2}}, \qquad (47)$$

then satisfy

$$b\, v_n = -\kappa, \qquad (48a)$$

with

$$b = \frac{2K}{\gamma M} = -\frac{2}{\gamma}\frac{\langle u_0\prime(Z), u_0\prime(Z)\rangle}{\langle u_0(Z), \widetilde{\mathfrak{D}}^{\gamma}_{|Z|} u_0(Z)\rangle} \tag{48b}$$

and

$$K\, v_n = -\frac{1}{2}\gamma\, M\kappa. \tag{48c}$$

Note that for normal diffusion ($\gamma = 2$) $b = 1$.

4.2. Numerical simulation

By (48c), a circular spot with $u = 1$ for $r > R(t)$ and $u = -1$ for $r < R(t)$ will collapse so that $R^2(t) = R_0^2 - \alpha t$ with $\alpha = \text{const}$. Numerical solution of (43) with an initial condition corresponding to a circular spot allowed to measure the collapse rate directly. Figure 12 presents the collapsing spot at several time instants for $\gamma = 1.5$ and the quantity $R^2(t;\gamma)$, depending linearly on time in accordance with (48c) (see comparison of numerical and analytically predicted values of α in the table).

Results of a numerical solution of (43) with $\gamma = 1.5$ and random initial data are depicted in figure 13(a). During the early stage of the evolution a domain structure is formed, followed by a gradual coarsening until a single spot remains and collapses. The average size of the structure was computed as

$$\langle L\rangle = \frac{1}{2}\left(\langle L_x\rangle + \langle L_y\rangle\right), \quad \langle L_\eta\rangle = \frac{\mathrm{L}_D}{\mathrm{N}_p}\sum_{\eta}\frac{1}{N_\eta}, \tag{49}$$

with $\langle L_\eta\rangle$ being the structure size in direction η, N_η - the number of zeros in that direction, L_D - the domain length (square) and N_p - the number of division points. Figure 13(b) shows the curves $\langle L\rangle(t)$ for several values of γ. During the domain structure formation $\langle L\rangle \sim t^{1/\gamma}$, followed by the crossover to the domain coarsening slightly slower than $\langle L\rangle \sim t^{1/2}$ and similar for all γ. At the very late stage, when there is only one spot left, there is a slight acceleration of coarsening to the rate $\langle L\rangle \sim t^{1/2}$ for all γ.

5 Phases with distinct Lyapunov functional densities

The specific feature of model (1) is the energetic equivalence of the phases $u_\pm = \pm 1$, characterised by the equal densities of Lyapunov functional

$$U(u) = -\frac{1}{4}\left(1 - u^2\right)^2. \tag{50}$$

Since $U(u_+) = U(u_-)$, a flat domain wall between the phases is stationary. Consider another potential $U(u)$ with two stable states $U'(u_+) = U'(u_-) = 0$, $U''(u_\pm) > 0$ such that $U(u_+) > U(u_-)$. Then according to (2b), the front between u_+ and u_- will move so that the state u_+ will oust the state u_-. Propagation of the front with constant velocity is governed by the function $u = u(z)$, $z = x - ct$, satisfying

$$\mathfrak{D}^{\gamma}_{|z|} u + c\frac{du}{dz} + U'(u) = 0 \tag{51}$$

	α_{num}	α_{th}
$\gamma = 2.0$	2.04	2.0
$\gamma = 1.5$	3.14	3.22
$\gamma = 1.0$	8.34	8.55

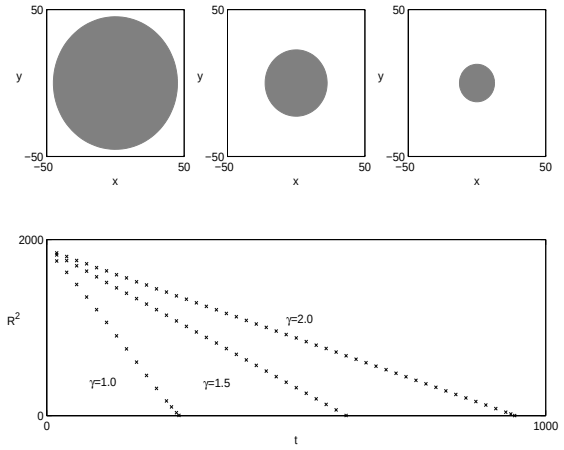

Figure 12: A circular spot collapse: time evolution for $\gamma = 1.5$ (upper, left to right) and $R^2(t;\gamma)$ (lower). For collapse rate $\alpha(\gamma)$ see the table.

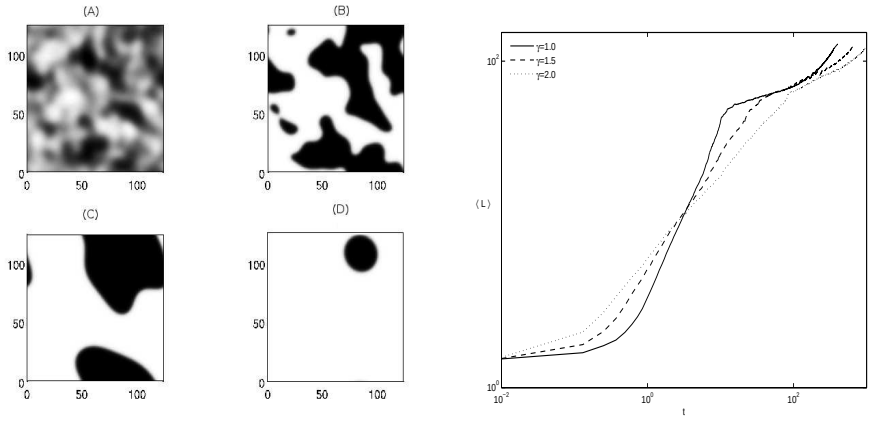

(a) Coarsening field for $\gamma = 1.5$: initial domain structure formation (A); intermediate coarsening stages (B-C); latest coarsening stage – a single collapsing spot (D).

(b) Coarsening rates for several values of γ.

Figure 13: Two dimensional coarsening properties.

with the boundary conditions $u(\mp\infty) = u_\pm$. As an example, consider the potential

$$U(u) = -\frac{1}{4}\left(1-u^2\right)^2 + \epsilon\mu u, \quad 0 < \epsilon \ll 1, \quad 0 < \mu \sim O(1) \tag{52}$$

and the domain wall solution

$$u(x,t) = u_0(x - \xi(\tau)) + \epsilon u_1(x) + o(\epsilon^2), \quad \tau = \epsilon t. \tag{53}$$

Substituting (52) and (53) into (3a) and collecting terms of order $O(\epsilon^0)$,

$$\mathfrak{D}^\gamma_{|x|} u_0 + u_0 - u_0^3 = 0. \tag{54}$$

Hence u_0 is the stationary domain wall solution of the fractional Allen-Cahn equation discussed previously. At order $O(\epsilon)$ a non-homogeneous equation is obtained:

$$\mathfrak{D}^\gamma_{|x|} u_1 + (1 - 3u_0^2)u_1 = \mu + \partial_x u_0 \, \frac{d\xi}{d\tau}. \tag{55}$$

The solvability condition (orthogonality of the right-hand side to the homogeneous problem solution $\partial_x u_0$) gives

$$K\frac{d\xi}{d\tau} = -2\mu \tag{56a}$$

with

$$K = \int_{\mathbb{R}} \left(\partial_x u_0\right)^2 dx \tag{56b}$$

being the inverse domain wall mobility. Relation (56) holds also for a domain wall with $u(\mp\infty) = u_\pm$.

For a pair of interacting domain walls of different sign the following conditions are obtained (see section *3.1.*)

$$K\frac{d\xi_1}{d\tau} = -2\mu + \alpha(\xi_2 - \xi_1)^{-\gamma}, \tag{57a}$$

$$K\frac{d\xi_2}{d\tau} = 2\mu - \alpha(\xi_2 - \xi_1)^{-\gamma}, \tag{57b}$$

with α constant. Such a pair describes a nucleus for a preferable phase $u \approx u_+$ in the sea of the phase $u = u_-$ (in the case $\mu > 0$). If the distance between the domain walls is

$$\xi_2 - \xi_1 = \ell_* = \left(\frac{\alpha}{2\mu}\right)^{1/\gamma}, \tag{58}$$

the nucleus boundaries are motionless (critical nucleus). Obviously, the critical nucleus is unstable: if $\ell < \ell_*$, the attracting force prevails and the nucleus disappears; otherwise it grows.

In the case of a curved front the velocity of the plane front $\pm 2\mu/b$ is added to the curvature flow velocity, hence (48c) becomes

$$K\, v_n = -\frac{1}{2}\gamma\, M\kappa + 2\mu, \tag{59}$$

where the normal is directed from the preferred phase with the lower Lyapunov density towards the phase with the higher one.

6 Conclusion

A fractional analogue of Allen-Cahn equation was formulated as a possible model for phase separation transition in media giving rise to super-diffusion of Lévy flight type. The equation can be obtained by a functional variation, and time dependent solutions decay to a stationary solution. Motivated by the normal $\tanh$ profile properties, odd stationary front-like solution was sought for different values of γ.

The variational formulation was utilised to generate the front profiles for three trial functions: a third degree polynomial, a sum of sines and a fifth degree odd polynomial, smoothly connected with an algebraically decaying tail, whose asymptotics were determined by Fourier transform method. The corresponding functional values and such global properties as slope at origin and wall mobility were compared with a direct numerical solution, rendering the third degree polynomial the best fit of the three.

The influence of diffusion anomaly on the dynamics of domain walls was analysed for plane and curved fronts between states with identical and different Lyapunov densities. In particular, a γ-dependent relation between the front normal velocity and curvature was formulated, generalising the expressions known for normal diffusion.

The effect on the coarsening phenomenon was predicted in the case of plane fronts, and the approach velocity of adjacent kinks was shown to be a power law of their distance. Simulations with random initial data in one and two spatial dimensions revealed the coarsening rates at the various evolution stages: $t^{1/\gamma}$ during formation of domain structures followed by kink or spot annihilation as $t^{1/2}$. A simulation with the special initial condition of a circular spot yielded a good accordance of numerical and theoretical results.

Thus, the introduction of a non-local diffusion operator has resulted in (i) a power law description of a plane front tail and approach velocity of two kinks rather than a normally exponential function; (ii) γ-dependent global properties such as front slope at the origin, domain wall mobility and coarsening rates for plane fronts, and proportionality factor between a curved front normal velocity and curvature.

Acknowledgements

A.A.N. acknowledges the support of the ISF grant #812/06 and Minerva Center for Nonlinear Physics of Complex Systems. A.A.G. acknowledges the support of the NSF grant #DMS-0707445.

A Inner layer equations of a curved front

Rewriting (43a) with the slow variables $X = \epsilon x$, $Y = \epsilon y$, $T = \epsilon^2 t$, and denoting $\Xi = \epsilon\xi$, $H = \epsilon\eta$,

$$\epsilon^2 u_T(X,Y,T) = -\epsilon^{\gamma+1} C_{2,\gamma/2} \int_{\mathbb{R}^2} \frac{[u(X,Y,T) - u(\Xi,H,T)]d\Xi dH}{[(X-\Xi)^2 + (Y-H)^2]^{(2+\gamma)/2}} + u - u^3. \tag{A1}$$

Defining the inner layer coordinate $z = (Y - h(X,T))/\epsilon$ and correspondingly $\zeta = (H - h(X,T))/\epsilon$,

$$\epsilon^2 \left(u_T - \frac{1}{\epsilon} h_T u_z \right) = -\epsilon^{\gamma+1} C_{2,\gamma/2} \times \tag{A2}$$

$$\int_{\mathbb{R}^2} \frac{[u(X,Y,T) - u(\Xi,H,T)] d\Xi dH}{\left[(X-\Xi)^2 + (h(X,T) - h(\Xi,T) + \epsilon(z-\zeta))^2 \right]^{(2+\gamma)/2}} + u - u^3.$$

Since $X - \Xi \sim O(\epsilon)$ and $h(X,T) - h(\Xi,T) \sim O(\epsilon)$, define $\Xi - X = \epsilon\xi$ and expand

$$h(X,T) - h(\Xi,T) \sim -\epsilon h_X(X,T)\xi - \frac{1}{2}\epsilon^2 h_{XX}(X,T)\xi^2 + O(\epsilon^3), \tag{A3a}$$

$$u(X,z,T) - u(\Xi,\zeta,T) \sim u(X,z,T) - u(X,\zeta,T) - \epsilon u_X(X,\zeta,T)\xi + O(\epsilon^2). \tag{A3b}$$

Now

$$\epsilon^2 u_T - \epsilon h_T u_z = -C_{2,\gamma/2} \times$$

$$\int_{\mathbb{R}^2} \frac{[u(X,z,T) - u(X,\zeta,T) - \epsilon u_X(X,\zeta,T) + O(\epsilon^2)] d\xi d\zeta}{\left[\xi^2 + (-h_X\xi + z - \zeta - \frac{1}{2}\epsilon h_{XX}\xi^2 + O(\epsilon^2))^2 \right]^{(2+\gamma)/2}} + u - u^3. \tag{A4}$$

The problem to leading order

$$-C_{2,\gamma/2} \int_{\mathbb{R}^2} \frac{[u_0(X,z,T) - u_0(X,\zeta,T)] d\xi d\zeta}{[\xi^2 + (-h_X\xi + z - \zeta)^2]^{(2+\gamma)/2}} + u_0 - u_0^3 = 0 \tag{A5}$$

reduces to

$$\left(1 + h_X^2\right)^{\gamma/2} \widetilde{\mathfrak{D}}^{\gamma}_{|z|} u_0 + u_0 - u_0^3 = 0, \quad u_0 = u_0(X,z,T), \tag{A6}$$

where $\widetilde{\mathfrak{D}}^{\gamma}_{|z|}$ (a single dimensional version of (43b)) is equivalent to the fractional operator defined in (4). Due to the property $\mathfrak{D}^{\gamma}_{|z|} f(z) = \delta^{\gamma} \mathfrak{D}^{\gamma}_{|\delta z|} f(\delta z)$ equation (A6) is solved as

$$u_0(X,z,T) = u_{pf}\left(\frac{z}{\sqrt{1+h_X^2}} \right) \tag{A7}$$

with u_{pf} being the plane front (13). Retaining terms of order $O(\epsilon)$ in (A4),

$$-\epsilon h_T\, u_z = \left(1 + h_X^2\right)^{\gamma/2} \widetilde{\mathfrak{D}}^{\gamma}_{|z|} u + u - u^3 + \frac{\epsilon\, C_{1,\gamma/2}\; h_X}{\left(1 + h_X^2\right)^{1-\gamma/2}} \int_{\mathbb{R}} u_X(X,\zeta,T) s_\gamma(\zeta) d\zeta -$$

$$\frac{\epsilon\, C_{2,\gamma/2}(\gamma+2) h_{XX}}{2\left(1+h_X^2\right)^{2-\gamma/2}} \int_{\mathbb{R}^2} \frac{u(X,z,T) - u(X,\zeta,T)}{\left(1+\tilde{\xi}^2\right)^{2+\gamma/2}} \left(\tilde{\xi}^2(1 - 2h_X^2) + h_X^2 \right) s_\gamma(\zeta) d\tilde{\xi} d\zeta, \tag{A8a}$$

$$s_\gamma(\zeta) = \frac{\mathrm{sign}(z-\zeta)}{|z-\zeta|^\gamma}, \quad \tilde{\xi} = \frac{1+h_X^2}{|z-\zeta|}\,\xi - h_X \mathrm{sign}(z-\zeta). \tag{A8b}$$

Scrutiny of the first integral on the right-hand side allows to write

$$I_1 := -C_{1,\gamma/2}\int_{\mathbb{R}} u_X(X,\zeta,T)s_\gamma(\zeta)d\zeta =$$

$$C_{1,\gamma/2}\int_{\mathbb{R}} \left(u_X(X,z,T)-u_X(X,\zeta,T)\right)s_\gamma(\zeta)d\zeta, \tag{A9}$$

with subsequent differentiation yielding

$$I_1 = \gamma\,\partial_z^{-1}\widetilde{\mathfrak{D}}^\gamma_{|z|}u_X(X,z,T). \tag{A10}$$

Completing the integration over $\tilde{\xi}$ in the second integral gives

$$I_2 := C_{2,\gamma/2}\int_{\mathbb{R}^2}\frac{u(X,z,T)-u(X,\zeta,T)}{\left(1+\tilde{\xi}^2\right)^{2+\gamma/2}}\left(\tilde{\xi}^2(1-2h_X^2)+h_X^2\right)s_\gamma(\zeta)d\tilde{\xi}d\zeta =$$

$$\frac{\gamma}{2+\gamma}\left(1-2h_X^2+(1+\gamma)h_X^2\right)\partial_z^{-1}\widetilde{\mathfrak{D}}^\gamma_{|z|}u(X,z,T). \tag{A11}$$

Substituting $u = u_0+\epsilon u_1+O(\epsilon^2)$ into (A8a) and extracting the problem for u_1,

$$\left(\left(1+h_X^2\right)^{\gamma/2}\widetilde{\mathfrak{D}}^\gamma_{|z|}+1-3u_0^2\right)u_1 = -h_T u_{0z}+\gamma\left(1+h_X^2\right)^{\gamma/2-1}\times$$

$$\left(h_X\partial_z^{-1}\widetilde{\mathfrak{D}}^\gamma_{|z|}u_{0X}+\frac{h_{XX}}{2\left(1+h_X^2\right)}\left(1+(\gamma-1)h_X^2\right)\partial_z^{-1}\widetilde{\mathfrak{D}}^\gamma_{|z|}u_0\right). \tag{A12}$$

Differentiating (A6) with respect to z gives the homogeneous solution $u_{1hom} = \partial_z u_0$. Hence by Fredholm alternative a solution for u_1 exists if the right-hand side of (A12) is orthogonal to u_{1hom}. A few auxiliary identities to be used are

$$\langle\partial_z u_0,\partial_z u_0\rangle = \left(1+h_X^2\right)^{-1/2}\int_{\mathbb{R}} {u_0}'^2(Z)dZ,\quad Z = z\left(1+h_X^2\right)^{-1/2}, \tag{A13a}$$

$$\langle\partial_z u_0,\partial_z^{-1}\widetilde{\mathfrak{D}}^\gamma_{|z|}u_0\rangle = -\langle u_0,\widetilde{\mathfrak{D}}^\gamma_{|z|}u_0\rangle, \tag{A13b}$$

$$\langle\partial_z u_0,\partial_z^{-1}\widetilde{\mathfrak{D}}^\gamma_{|z|}u_{0X}\rangle = -\frac{1}{2}\frac{\partial}{\partial X}\left(u_0\widetilde{\mathfrak{D}}^\gamma_{|z|}u_0\right). \tag{A13c}$$

Equality (A13b) ensues by partial integration and asymptotics of $\widetilde{\mathfrak{D}}^\gamma_{|z|}u_0 = u_0(u_0^2-1)\sim|z|^{-\gamma}$ at infinity due to (13). Equality (A13c) follows since $\widetilde{\mathfrak{D}}^\gamma_{|z|}$ is self adjoint. Defining

$$K := \int_{\mathbb{R}} {u_0}'^2(Z)dZ,\quad M := -\int_{\mathbb{R}} u_0(Z)\widetilde{\mathfrak{D}}^\gamma_{|Z|}u_0(Z)dZ, \tag{A14}$$

the solvability condition of (A12) is given by

$$K\,h_T = \frac{1}{2}\gamma\,M\frac{h_{XX}}{1+h_X^2}. \tag{A15}$$

Introducing the normal velocity v_n and the front curvature κ

$$v_n = \frac{h_T}{\sqrt{1+h_X^2}}, \quad \kappa = -\frac{h_{XX}}{(1+h_X^2)^{3/2}}, \tag{A16}$$

it is found that

$$b\, v_n = -\kappa, \tag{A17a}$$

where

$$b = \frac{2K}{\gamma M} = -\frac{2}{\gamma}\frac{\langle u_0\prime(Z), u_0\prime(Z)\rangle}{\langle u_0(Z), \widetilde{\mathfrak{D}}^{\gamma}_{|Z|} u_0(Z)\rangle} \tag{A17b}$$

and

$$K\, v_n = -\frac{1}{2}\gamma\, M\kappa. \tag{A17c}$$

References

[1] Pismen L M 2006 *Patterns and interfaces in dissipative dynamics* (Berlin: Springer)

[2] Murray J D 1993 *Mathematical biology* (Berlin: Springer)

[3] Pelcé P (Ed.) 1988 *Dynamics of curved fronts* (Boston: Academic Press).

[4] Allen S M and Cahn J W 1979 A microscope theory for antiphase boundary motion and its application to antiphase domain coarsening *Acta Metall.* **27**(6) 1085–1095

[5] Fisher R A 1937 The wave of advance of advantageous genes *Ann. Eugenics* **7** 355–369

[6] Kolmogoroff A N, Pertrovsky I G and Piscounoff N S 1937 Study of the diffusion equation with growth of the quantity of matter and its application to a bilogical problem *Moscow Uni., Bull. Math.* **1** 1–25

[7] Balk A M 2002 Anomalous behaviour of a passive tracer in wave turbulence *J. Fluid Mech.* **467** 163–203

[8] Meerschaert M M and Tadjeran C 2004 Finite difference approximations for fractional advection – dispersion flow equations *J. Comput. Appl. Math.* **172** 65–77

[9] Viswanathan G M, Afanasyev V, Buldyrev S V, Murphy E J, Prince P A and Stanley H E 1996 Lévy flight search patterns of wandering albatrosses *Nature* **381** 413–415

[10] Metzler R and Klafter J 2000 The random walk's guide to anomalous diffusion: a fractional dynamics approach *Phys. Rep.* **339**(1) 1–77

[11] Klafter J, Zumofen G and Shlesinger M F, in: Mallamace F and Stanley H E (Eds.) 1997 *The Physics of complex systems* (Amsterdam: IOS Press)

[12] Mancinelli R, Vergni D and Vulpiani A 2002 Superfast front propagation in reaction systems with anomalous diffusion *Europhys. Lett.* **60** 532

[13] del Castillo-Negrete D, Carreras B A and Lynch V E 2003 Front dynamics in reaction – diffusion systems with Lévy flights: a fractional diffusion approach *Phys. Rev. Lett.* **91**(1) 018302

[14] Brockmann D and Hufnagel L 2007 Front propagation in reaction - superdiffusion dynamics: taming Lévy flights with fluctuations *Phys. Rev. Lett.* **98** 178301

[15] Hinrichsen H 2007 Non-equilibrium phase transitions with long-range interactions *J. Stat. Mech.: Theor. Exp.* **07** P07006

[16] Frontera C, Vives E and Planes A 1993 Monte Carlo study of the relation between vacancy diffusion and domain growth in two-dimensional binary alloys *Phys. Rev. B* **48**(13) 9321–9326

[17] Marini Bettolo Marconi U 1998 Interface pinning and slow ordering kinetics on infinitely ramified fractal structures *Phys. Rev. E* **57**(2) 1290–1301

[18] Podlubny I 1994 *The Laplace transform method for linear differential equations of the fractional order*, Košice, Slovenská Republika.

[19] Kawasaki K and Ohta T 1982 Kink dynamics in one-dimensional non-linear systems *Physica A* **116**(3) 573–593

[20] Nagai T and Kawasaki K 1983 Molecular dynamics of interacting kinks. I *Physica A* **120**(3) 587–599

[21] Bogdan K, Kulczycki T and Kwaśnicki M 2008 Estimates and structure of α-harmonic functions *Probab. Theory Relat. Fields* **140** 345–381